Accepted manuscript doi:

10.1680/jgeot.23.00498

Accepted manuscript doi:
10.1680/jgeot.23.00498

Submitted: 15 December 2023

Published online in 'accepted manuscript' format: 03 October 2024

Manuscript title: Re-examination and analysis of test data on consolidation of soft soils exhibiting creep with different thicknesses

Authors: Pei-Chen Wu[*], Ze-Jian Chen[*], Jian-Hua Yin[*], Yoichi Watabe[†], Ding-Bao Song[*] and Peng-Lin Li[*]

Affiliations: [*]Department of Civil and Environmental Engineering, The Hong Kong Polytechnic University, Hong Kong Special Administrative Region, China [†]Laboratory of Soil Mechanics, Division of Civil Engineering, Faculty of Engineering Hokkaido University, Sapporo, Japan

Corresponding author: Ze-Jian Chen, Department of Civil and Environmental Engineering, The Hong Kong Polytechnic University, Hong Kong Special Administrative Region, China

E-mail: watabe@eng.hokudai.ac.jp

Accepted manuscript doi:
10.1680/jgeot.23.00498

Abstract

Accurate prediction on long-term settlements of soft soils is challenging. One of the reasons is the time-dependent soil behaviours. How to extrapolate such behaviours from thin laboratory testing with limited time scales to in situ thick soil layer with large time scales is still an ongoing debate, which can be dated back to Ladd *et al*. (1977). Many experimental results previously used to advocate Hypothesis A have been re-analysed and found to align with Hypothesis B. However, discrepancies remain in some historical data, particularly in the case of Osaka clay retrieved from the seabed under the Kansai International Airport Islands. This study begins by introducing the main implications and selected existing models for the time-dependent behaviours of soft soil. It then focuses on the re-examination of selected testing results from Watabe *et al*. (2008b), supplemented by numerical simulation using isotache models. The analysis emphasises the importance of considering equal initial conditions when comparing data from samples with varying thicknesses. Furthermore, the good agreement observed between measured data and the simulation results using Hypothesis B methods demonstrates the validity of Hypothesis B for predicting the long-term consolidation behaviour of soft soil in both laboratory and field scales.

Keywords: clays, compressibility, creep, isotache models, settlement

Accepted manuscript doi:
10.1680/jgeot.23.00498

Introduction

Depending on the soil type, classical Terzaghi's consolidation theory with or without the consideration of secondary compression (creep) is commonly used in routine geotechnical practice. However, accurate prediction on long-term settlement, particularly for soft soil, can be extremely challenging. One of the well-known projects suffering from long-term settlement is the Kansai International Airport, which was constructed on a large reclaimed land in Osaka Bay (Watabe *et al*., 2008a). The actual settlement of the Kansai International Airport was significantly larger than the designed value, which has attracted the attention of many scholars and geotechnical engineers on long-term settlement prediction (Rocchi *et al*., 2006, 2007; Funk *et al*., 2013; Mesri & Funk, 2015).

Ladd *et al*. (1997) raised a fundamental question on whether creep acts as a separate phenomenon while excess pore pressure dissipates during primary consolidation. Since then, an ongoing debate has been revolved, focusing on extrapolating the time-dependent behaviours of soft soil from thin laboratory testing with limited time scales to in situ thick soil layer with large time scales (Mesri, 2003; Augustesen *et al*., 2004; Leroueil, 2006; Degago *et al*., 2011; Yin & Feng, 2017; Chen *et al*., 2021; Liu & Borja, 2022).

Ladd et al. (1977)'s hypotheses

Two extreme curves are plotted in Fig. 1 to illustrate the effect of sample thickness. According to Ladd's explanations, assuming B-type curves is to advocate that creep acts as a separate phenomenon (structural viscosity creep mechanism) during the primary consolidation, while assumption of A-type curves is commonly used in practice.

Jamiolkowski et al. (1985)'s hypotheses

Jamiolkowski *et al*. (1985) provided a more straightforward definition of Hypotheses A and B. In their definition, Hypothesis A assumes the creep occurs only after the end of primary consolidation (EOP), whereas Hypothesis B considers creep occurring during and after primary consolidation.

Although both Ladd and Jamiolkowski's definitions of Hypothesis A predict a unique EOP strain (or void ratio) independent of sample thickness, Jamiolkowski's assumption of nonexistence of creep during primary consolidation for Hypothesis A is misleading. Later, the main advocators of Hypothesis A clarified that creep does occur during primary consolidation but depends on

degree of primary consolidation (Mesri & Choi, 1985; Mesri, 1995). Nevertheless, the argument on Hypotheses A and B should focus on whether the uniqueness of EOP void ratio-effective stress relationship stays true or not (Szavits-Nossan, 2015; Mesri & Kane, 2018), instead of the commencement of creep.

There have been many laboratory and field test results that have contributed to advocating each hypothesis (Berre & Iverson, 1972; Mesri & Choi, 1985; Imai & Tang, 1992; Watabe *et al*., 2008b; Degago *et al*., 2009; Gheisari *et al*., 2023). By reanalysing those test results, Degago *et al*. (2011) found out that some results that have been previously used to advocate Hypothesis A turn out to support Hypothesis B. However, contradictions still appear, particularly for those samples showing both Hypotheses A- and B-like behaviours, for instance, Osaka Bay clay reported in Watabe *et al*. (2008b). Unlike conventional isotache models, Yuan & Whittle (2018) formulated a different elasto-viscoplastic (EVP) model for describing the time-dependent behaviours of soil, by introducing an internal state variable. This model aimed to provide a mathematical framework for both Hypotheses A and B. However, their prediction for Hypothesis A might be applicable to sandy soils but may not hold true for clay.

In this paper, the main implications and selected existing models for time-dependent behaviours of soft soil are reviewed first. The focus is then given to the re-examination of selected testing results from Watabe *et al*. (2008b), along with numerical simulation to emphasise that the equal initial conditions should not be overlooked when comparing the data results from the samples with various thickness. Selected successful cases of settlement predictions using Hypothesis B methods are summarized at the end of the paper.

SELECTED EXISTING MODELS

There are many existing models for investigating the creep of soil, including those based on Hypothesis A framework (Mesri & Tane, 2018; Mesri & Funk, 2015), constitutive models based on isotache framework (Yin & Graham, 1989, 1996; Vermeer & Neher, 1999; Leroueil, 2006; Watabe *et al*., 2008a, 2012; Watabe & Leroueil, 2015), non-isotache EVP models (Yuan, 2016; Yuan & Whittle, 2018), and hyper-viscoplastic models deducted from thermodynamics point of view (Aung *et al*., 2019; Grimstad *et al*., 2020; Dadras-Ajirloo *et al*., 2023 and 2024). In this study, the focus is on Mersi's theory, Vermeer and Neher's Soft Soil Creep (SSC) model as a representative of isotache framework, and Yuan and Whittle's EVP model as a representative of non-isotache framework.

Mesri's theory

The main ideas provided by Mesri and his colleagues for long-term behaviour of soft soil are based on two assumptions, namely (1) uniqueness of the EOP void ratio-effective vertical stress relationship and (2) C_α/C_c law of compressibility. The one-dimensional compression behaviour of soft soil is expressed as

$$\frac{de}{dt}=\left(\frac{\partial e}{\partial \sigma_v'}\right)_t \frac{\partial \sigma_v'}{\partial t}+\left(\frac{\partial e}{\partial t}\right)_{\sigma_v'} \tag{1}$$

where $\left(\partial e/\partial \sigma_v'\right)_t$ and $\left(\partial e/\partial t\right)_{\sigma_v'}$ refer to "stress compressibility" and "time compressibility", respectively. Despite the values of $\left(\partial e/\partial t\right)_{\sigma_v'}$ during primary consolidation being related to primary consolidation duration t_p, Mesri and Kane (2018) claimed that the difference in consolidation duration and effective stress rate existing between thin and thick soil samples balances the contribution of stress and time compressibility. This, in turn, results in an EOP void ratio-effective vertical stress relationship independent of the consolidation period. In addition, they considered that vertical strain rate at EOP is expressed as:

$$\dot{\varepsilon}_{EOP}=\frac{k_{v0}}{2^{C_c/C_k}H^2}\frac{\bar{\sigma}_p'}{\gamma_w}\frac{C_\alpha}{C_c} \tag{2}$$

where k_{v0} is in situ coefficient of permeability; $C_k=\Delta e/\Delta \log k_v$; $\bar{\sigma}_p'$ refers to pre-consolidation pressure; H is the maximum drainage distance.

Based on Eqs. (1) and (2), Mesri and his colleagues developed a program called ILLICON for settlement evaluation (Mesri & Funk, 2015). However, it is considered that the theoretical

validity of Mesri's assumption regarding the balance between time- and stress compressibility components requires further investigation.

Isotache models

Phenomenological relations among void ratio e (or strain ε), change rate of void ratio $\dot{e}$ or time t, and effective stress σ'_v have been widely studied (Šuklje, 1957; Bjerrum, 1967; Garlanger, 1972). The formations for conceiving the unique relation of $e-\dot{e}-\sigma'_v$ are called isotache models, advocating Hypothesis B (Yin & Graham, 1989, 1996; Vermeer & Neher, 1999; Leroueil, 2006; Watabe *et al*., 2008a, 2012; Watabe & Leroueil, 2015).

In many isotache models, such as Vermer & Neher's SSC model and Yin and Graham's EVP model, the total strain rate is composited of elastic strain rate and viscoplastic strain rate:

$$\dot{\varepsilon} = \dot{\varepsilon}^e + \dot{\varepsilon}^{vp} \tag{3}$$

In one dimensional SSC model, elastic strain rate can be expressed as:

$$\dot{\varepsilon}^e = \frac{\kappa^*}{2}\left(\frac{\dot{\sigma}'_v}{\sigma'_v}\right) \tag{4}$$

where $\kappa^* \approx 2\kappa/V$ is the modified swelling index; κ is the slope of un/reloading line; $V = 1+e_0$ is the specific volume.

And creep (viscoplastic) strain rate $\dot{\varepsilon}^{vp}$ can be expressed as:

$$\dot{\varepsilon}^{vp} = \frac{\mu^*}{\tau}\left(\frac{\sigma'_v}{\sigma'_{pp}}\right)^{\frac{\lambda^*-\kappa^*}{\mu^*}} \tag{5}$$

where $\lambda^* = \lambda/V$ and μ^* are the modified compression and creep indices, respectively; λ is the slope of normally consolidation line; σ'_{pp} refers to the pre-consolidation pressure which changes as soil compresses, as illustrated in Fig.2. $\tau = 1\,\text{day}$ has a similar meaning as the

reference time defined by Yin & Graham (1989 and 1994). Song *et al*. (2024) demonstrated that SSC model is equivalent to Yin & Graham's elastic viscoplastic (EVP) model. Nonlinear creep and a concept of limited time line (limited creep) were later introduced to Yin and Graham's EVP model to provide more accurate prediction on long-term settlement (Yin, 1999; Chen *et al*., 2021). Most recently, Hypothesis B methods based on Yin and Graham's EVP model for settlement calculation have been adopted in the 5th edition of Canadian Foundation Engineering Manual (Canadian Geotechnical Society, 2023).

Non-isotache EVP model

Yuan (2016) and Yuan & Whittle (2018) developed a different EVP model (MIT-SR model) by introducing an internal variable. Similar to SSC model, the total strain rate is comprised of elastic strain rate and viscoplastic strain rate in MIT-SR. The elastic strain rate is expressed as:

$$\dot{\varepsilon}^{e} = \rho_r n \frac{\dot{\sigma}'_v}{\sigma'_v} \tag{6}$$

where ρ_r is the slope of the unloading/reloading line in log(e)-log(σ'_v) space, as shown in Fig. 2; $n = \frac{e}{1+e}$ is soil porosity. Different from aforementioned isotache models, MIT-SR model considers that viscoplastic strain rate of soils is not only dependent on the current effective stress and void ratio state, but also influenced by the memory of the soil skeleton. Furthermore, MIT-SR model is capable of simulating non-isotache behaviour, such as overshooting and transient effect, observed in constant rate of strain (CRS) tests on sandy soil (Levin *et al*., 2019). The viscoplastic strain rate is expressed as:

$$\dot{\varepsilon}^{vp} = R_a \left(\frac{\sigma'_v}{\sigma'_p} \right) \tag{7}$$

where R_a is called "internal strain rate", corresponding to the overall perturbation of the soil particle assembly (memory of the soil skeleton); σ'_p is a reference stress defined on limiting compression curve (LCC), for which the following hardening rule is applied.

$$\dot{\sigma}'_p = \frac{\sigma'_p}{\rho_r n} \dot{\varepsilon} \tag{8}$$

Yuan & Whittle (2018) adopted an "activation and decay" mechanism to describe the relation between the "internal strain rate", R_a, and total strain rate, $\dot{\varepsilon}$, as expressed in Eq. (9).

$$\dot{R}_a = \left[f(\dot{\varepsilon}) - R_a \right] m_t \tag{9}$$

$$f(\dot{\varepsilon}) = \frac{\rho_c - \rho_r}{\rho_c} \dot{\varepsilon} \left(\frac{\dot{\varepsilon}}{\dot{\varepsilon}_{ref}} \right)^{-\beta} \tag{10}$$

$$m_t = \left(\frac{\rho_c}{\rho_\alpha} - 1 \right) \frac{\dot{\varepsilon}^{vp}}{\rho_r n} + \dot{\varepsilon} \tag{11}$$

where m_t is used for the consideration of transient effect; ρ_c is the slope the limiting LCC line in log(e)-log(σ'_v) space, as shown in Fig. 2; ρ_α is a material constant for the creep behaviour; $\dot{\varepsilon}_{ref}$ refers to a reference strain rate; β refers to the rate sensitivity, which is determined from CRS tests with different strain rates. The values of ρ_c, ρ_r, and ρ_α can be related to parameters λ^*, κ^*, and μ^* in SSC model, as shown in the notes of Table 2. While the new parameter in MIT-SR model, β, is not considered in SSC model.

R_a evolves from R_{a0} to $f(\dot{\varepsilon})$. When $R_a = f(\dot{\varepsilon})$, "steady state" is reached. Despite that MIT-SR model is not developed based on isotache framework, this model is equivalent to an isotache model when steady state is reached.

In the steady state, the total strain rate, $\dot{\varepsilon}$, and viscoplastic strain rate, $\dot{\varepsilon}^{vp}$, fulfil the following relation:

$$\dot{\varepsilon} = \frac{\rho_c}{\rho_c - \rho_r} \dot{\varepsilon}^{vp} \tag{12}$$

Combining Eqs. (10), (11), and (12), the relation between the viscoplastic strain rate, $\dot{\varepsilon}^{vp}$, and the vertical stress, σ'_v, in the steady state is expressed as:

$$\sigma'_v = \left(\frac{\rho_c}{\rho_c - \rho_r} \frac{\dot{\varepsilon}^{vp}}{\dot{\varepsilon}_{ref}} \right)^{\beta} \sigma'_p \tag{13}$$

or

$$\dot{\varepsilon}^{vp} = \frac{\rho_c - \rho_r}{\rho_c} \dot{\varepsilon}_{ref} \left(\frac{\sigma'_v}{\sigma'_p} \right)^{\frac{1}{\beta}}, \ (\beta \neq 0) \tag{14}$$

In Yuan and Whittle's MIT-SR model, four parameters, namely R_{a0}, ρ_α, β, and $\dot{\varepsilon}_{ref}$, are related to soil creep. ρ_α, $\dot{\varepsilon}_{ref}$ can be determined from IL oedometer test; β can be determined from CRS tests with different strain rates. Yuan and Whittle (2018) provided the following methods to estimate the value of R_{a0}:

(1) For OCR >2, $R_{a0} = 0$

(2) Ground monitoring of creep settlement before loading

(3) By assuming 99% consolidation of previous stage, and $R_{a0} \approx \dot{\varepsilon}_0^{vp} \approx \frac{0.434 C_\alpha}{(1+e) t_{99}} = \frac{\rho_\alpha n}{t_{99}}$.

$t_{99} = \frac{H^2}{c_v} T_{99}$ ($T_{99} \approx 1.78$) is corresponding to the time at 99% degree of consolidation.

However, Method (2) ground monitoring is unrealistic, especially for non-uniform soil profile and the use of t_{99} in Method (3) is over-simplified and many cause large error. Therefore, it is believed that determination of R_{a0} is one of the major issues of MIT-SR model.

The comparison between and MIT-SR model and SSC model is shown in Table 1.

If $\beta = 0$ and particular values of R_{a0}, for example $R_{a0} \propto \frac{1}{H^2}$, are used, MIT-SR can produce a unique EOP strain and overlapped *e*-logσ curves during primary consolidation, in other words, Hypothesis A behaviour. However, considering that β value is determined from CRS tests, $\beta = 0$ is unlikely to happen in clay samples but might be reasonable for sandy soil. Therefore, MIT-SR model does not support Hypothesis A, but rather provides a different time-dependent constitutive model suitable for both clayey and sandy soils. Nevertheless, the rate dependence has been found to be related to strain rate (Watabe & Leroueil, 2015).

Accepted manuscript doi:
10.1680/jgeot.23.00498

RE-EXAMINATION OF SELECTED TESTING DATA

Degago *et al*. (2009 and 2011) re-interpreted a series of test data that were used for supporting Hypothesis A. It was found that advocators of Hypothesis A misused isotache concept for total strain (or absolute void ratio) to compare with incremental strain (or change in void ratio), leading to incorrect conclusions regarding the time-dependent compressibility of clays. Using numerical simulation, Degago *et al*. (2011) further demonstrated that the predictions based on the isotache model agree well with the experimental observations.

Watabe *et al*. (2008b) investigated the consolidation behaviour of Osaka Bay mud in terms of total strain. In their observation, however, a special sample (Ma11) showed strain variations consistent with Hypothesis B for thin specimens, while following Hypothesis A for thick specimens. These discrepancies are possibly attributed to the unequal initial conditions. It is important to point out that any comparisons regarding Hypothesis A or B should be made under equal initial conditions and the same effective stress increment, which are demonstrated using the experimental results from Watabe *et al*. (2008b) as well as numerical simulations.

Experimental results from Watabe et al. (2008b)

Watabe *et al*. (2008b) designed and conducted a series of inter-connected type consolidation tests to study the relationship between soil thickness and long-term compression behaviour. In order to minimise the side friction between the soil specimen and the inner wall of the consolidation apparatus, thin soil elements were connected to form a thicker specimen. Both undisturbed (Ma11, Ma12, Ma13) and reconstituted (Ma13Re) soil samples were originally retrieved from the seabed of the Kansai International Airport. A hydraulically operated piston sampler was used to take undisturbed soil samples with good sample quality (Watabe *et al*., 2002). This paper aims to re-analyse the experimental results of Ma11, particularly specimens H2, H5, H10, and H20, by providing additional details on initial void ratios and simulating the long-term consolidation tests using SSC and MIT-SR models.

Ma11 clay samples were retrieved from a depth of -85 m, referenced to Chart Datum Level (CDL), with the overburden effective stress of 489 kPa, consolidation yield pressure of 701 kPa, over consolidation ratio (OCR) of 1.43, specific gravity of 2.67, liquid limit of 85.9%, plastic limit of 25.6%, plasticity index of 60.3%, and natural water content of 51.5%. The properties of other clay samples and detailed test conditions for the inter-connected consolidation tests can be found in Watabe *et al*. (2008b). H2, H5, H10, and H20 of Ma11 were formed by connecting two

10 mm-thick soil elements, five 10 mm-thick soil elements, five 20 mm-thick soil elements, and ten 20 mm-thick soil elements, respectively. For each specimen, preliminary consolidation (bypass drainage condition for 1 day and overburden effective stress of 489 kPa for 7 days) was conducted before the long-term consolidation test (target pressure of 1078 kPa) to ensure the loading condition similar to the real one in the subsoil layer related to the reclamation of the Kansai International Airport. Porewater pressure transducers were used to monitor the dissipation of excess porewater pressure of each specimen element during the long-term consolidation tests. The durations of long-term consolidation of H2, H5, H10, and H20 were 14.7, 15.7, 31.7, and 52.5 days, respectively. It should be noted that the test procedure in Watabe et al. (2008b) was not a true EOP test.

Fig. 3(a) plots the average strain-log(time) curves of specimens with different thickness. It should be noted that the plotted strains are incremental strains under the loading of the long-term consolidation test, which were used by Yuan & Whittle (2018) to demonstrate the versatility of their model for predicting both Hypotheses A and B behaviours. According to Degago *et al*. (2011), absolute (accumulated) strain should be plotted, as shown in Fig. 3(b). However, the accumulated strain of H5 still appears to be considerably greater than that of the other specimens. The comparisons among H2, H10, and H20 support Hypothesis B, while the comparison between H5 and H10 or H5 and H20 gives a Hypothesis A-like result.

Explanation by Watabe et al. (2008b)

Watabe et al. (2008b) believed that the thickness effect on the consolidation behaviour of Ma11 depended on the initial void ratio e_0 before the long-term consolidation test. By analysing the void ratio of H2, H5, and H10, they determined a boundary of $e_0 = 1.25$ to classify the specimen elements into two groups. They concluded that the value of $\Delta e / e_0$ increase with the thickness *H* for the specimen elements in $e_0 > 1.25$, while $\Delta e / e_0$ is nearly independent of the thickness *H* for those in e0<1.25. e_0 is the initial void ratio before the long-term consolidation test. $\Delta e = e_0 - e_{EOP}$ is the void ratio change during the primary consolidation. e_{EOP} refers to the void ratio at EOP, which is defined as 98% dissipation of the excess pore water pressure. It should be noted that the data of H20 was not presented in Watabe (2008b).

This study presents detailed data on void ratio for all four Ma11 specimens, H2, H5, H10, and H20, as shown in Fig. 4. It is considered that the classification regarding $e_0 = 1.25$ might be arbitrary. Furthermore, Fig. 5 presents relationship between $\Delta e / e_0$ and the maximum drainage

distance (thickness) of the specimens. Average values of $\Delta e / e_0$ for different specimens are marked in Fig. 5. It can be seen that if specimen H5 is not taken into account, the average value of $\Delta e / e_0$ increases with the thickness *H*, aligning with Hypothesis B.

Watabe *et al*. (2008b) mentioned that the soil sample might be heterogeneous because of some variation in the grain size distribution. Heterogeneity and distinct initial conditions could contribute to the differences observed among all the specimens. In addition, bedding error (non-perfect contact between the soil and piston) could be another possibility to cause the large strain (or $\Delta e / e_0$) of specimen H5. Specimens H2 and H5 consisted of two and five elements, respectively. Each element had the thickness of 10 mm. Specimens H10 and H20 consisted of five and ten elements, respectively. Each element had the thickness of 20 mm, as shown in Fig. 3(a). The bedding error for specimens H2 and H5 could be twice of that for specimens H10 and H20. It should be mentioned that the void ratio of each thin element of H5 was greater than that of H2, as shown in Fig. 4. Thus, the unreasonable larger strain of H5 could be attributed to the high initial void ratio and bedding error, while the influences of bedding error and void ratio might have been mitigated in the case of H2. As a result, it is considered that H5 should be excluded from the comparison.

Simulation by Yuan & Whittle (2018)'s MIT-SR model

Yuan & Whittle (2018) applied MIT-SR to simulate the long-term consolidation tests conducted by Watabe *et al*. (2008b). When $\beta = 0$, the MIT-SR model provided Hypothesis A-type curves. However, the simulated result only matched with specimen H5. For specimens H2, H10, and H20, the MIT model overestimated the vertical strains. When $\beta \neq 0$, the MIT-SR model provided Hypothesis B-type curves. The simulated result agreed well with the measured data for specimen H2. For specimens H5, H10, and H20, the MIT-SR model underestimated the vertical strains, as displayed in Fig. 9 of Yuan & Whittle (2018). It should be noted that the main issue of Yuan & Whittle (2018) is the way they manipulated the parameters to "fit" both Hypothesis A and B, which could be considered an improper use of the model. Apart from the determination of R_{a0}, the MIT-SR model has some interesting features.

In this study, MIT-SR model ($\beta \neq 0$) was implemented into COMSOL Multiphysics to simulate the long-term consolidation tests on Ma11 specimens H2, H10, and H20. The simulation results are plotted in Fig. 7 in terms of void ratio. The soil parameters used for the simulation are listed in Table 2. COMSOL Multiphysics is a commercial program that offers a user-friendly interface for solving partial differential equations using the finite element method.

Re-analyse using isotache model

Watabe's experimental data has been re-analysed using PLAXIS software, in which all soil specimens were simulated using SSC model under the axisymmetric condition. Considering the unneglectable differences between specimen H5 and the remaining specimens, specimen H5 was excluded from the numerical simulation.

According to the actual experiment setups, specimens H2, H10, and H20 were simulated using two (10 mm per layer), five (20 mm per layer), and ten (20 mm per layer) soil layers, respectively. Considering each soil element possessed a different initial void ratio, the actual initial void ratios from Watabe's experiment were assigned to the soil layers in PLAXIS. The loading schedule and time duration of each load increment in the simulation were the same as in the actual experiment, including both preliminary consolidation stage (overburden effective stress of 489 kPa) and long-term consolidation stage (target pressure of 1078 kPa). Table 2 lists the parameters used in MIT-SR model of Yuan & Whittle (2018) and SSC model in this paper.

Fig. 6 illustrates the relationship between initial void ratio and pre-consolidation pressure. Under the situation of identical initial vertical stress, the soil with a smaller initial void ratio tends to possess a larger pre-consolidation pressure. Therefore, the values of POP (pre-consolidation pressure) used in SSC model for each soil layer need to be modified according to the different values of initial void ratio. Table 3 lists the modified values of POP for specimen H2, H10, and H20. It is worth noting that if the input value of POP was taken as the reference value of 720 kPa, instead of the modified value adjusted based on the initial void ratio, SSC model would tend to overestimate the compression of the specimen element with the initial void ratio smaller than the average initial void ratio e_{0ave}. Mesri & Kane (2018) reassessed isotache compression concept and criticised it for overestimating EOP strain or void ratio. This overestimation could be also attributed to the incorrect interpretation of isotache models and used of incorrect values for POP or OCR and their corresponding initial void ratios in isotache models.

Fig. 7(a) presents measured and simulated void ratios versus time for different specimens using the actual values of the initial void ratio provided by Watabe *et al*. (2008b). The simulation results of H2, H10, and H20 agree well with the experimental results. The overall results on long-term consolidation behaviour of Ma11 predicted by SSC model are better than those predicted by MIT-SR model using the parameters presented in Table 2.

Fig. 7(b) presents the simulation results using both SSC and MIT-SR models assuming an identical initial void ratio for the specimens with different thicknesses. Clear Hypothesis B-type

curves appear, showing that the initial void ratio plays an important role in the predicted results. When the initial void ratios are different, which is usually the case for most of the laboratory and field data, the compression curves of thin and thick clay specimens (e.g., H10 and H20) might look like having similar EOP void ratio. However, those should not be considered to support Hypothesis A. Furthermore, those compression curves showing similar EOP void ratio can be well interpreted using isotache models, demonstrating the validity of Hypothesis B.

FIELD DATA

Based on the detailed information documented in Furudoi & Kobayashi (2009), Funk (2013) and Mesri & Funk (2015), Fig. 8 shows the subsoil profile from 0-140 m depth below seabed at MP1-II location of the Kansai International Airport. Sand piles were installed on a 2.5 m square grid in Ma 13 layer (Furudoi, 2010). Strictly speaking, the settlement prediction of Kansai International Airport Islands goes beyond the scope of 1D consolidation, considering the complicated sub-seabed profile, involving multi-layers of marine clays, non-marine clays, and sandwiched sand layers. Since this study focuses on Ma11 clay, SSC model was adopted to simulate the compression of Ma11 layer in PLAXIS without considering other soil layers. Fig. 8 illustrates the axisymmetric model of Ma 11 layer, which consists of three sublayers, namely Ma11 U1, Ma11 U2, and Ma11 L, with OCR = 1.43. Due to the presence of Ds3L and Ds5 sand layers above and beneath Ma 11 layer, the top and bottom boundaries of the axisymmetric model can be set as free drainage. Ds4 sand layer, sandwiched between Ma11U2 and Ma11L layers, was assumed to be incompressible. Therefore, Ds4 layer was not included in the axisymmetric model. The effective vertical stress on top of Ma 11 layer, σ'_v, can be determined by Eq. (15)

$$\sigma'_v = \sigma'_{vi} + \Delta\sigma'_v \tag{15}$$

where σ'_{vi} represents the effective vertical stress of 508 kPa on Ma 11 layer caused by the self-weight of the overlaying soil layers. $\Delta\sigma'_v$ represents the load at the seabed. Fig. 9(a) shows the simplified load used for the simulation. The maximum applied load on the seabed was 540 kPa, which, combined with the 508 kPa vertical stress from the self-weight of the overlying soil layers, resulted in a total effective vertical stress of 1048 kPa acting on the top of the Ma 11 layer for long-term consolidation analysis. Table 4 lists the main parameters used in the simulation. It should be noted that buoyance effects were not considered in the simulation.

As demonstrated in Fig. 9(b), the soil compression simulated using the SSC model agrees well with the measured field data, indicating the validity of the isotache model for field scale

simulation. It should be noted that this study only simulated the compression of Ma 11 layer rather than the total settlement of the seabed at MP1-II. Accurately simulating the total settlement of Kansai International Airport requires further in-depth studies to examine the properties and consolidation behaviours of all soil layers, including the marine soil layers, non-marine soil layers, and sand layers, as well as to perform the simulation with the consideration of 2D or 3D effects.

Fig. 10 provides a summary of surface settlement of embankments over soft soils and compression of soft soil at the end of observation for selected projects. The predicted settlements were calculated using Hypothesis B methods. For the case of tailings deposit, the predicted settlement was calculated using Yin & Graham's EVP model. The predicted settlements in other cases were calculated using SSC model. For the case of Osaka Bay, the predicted compression in Ma11 layer was calculated using SSC model. The predicted values agree well with the measured values, providing clear demonstration and validation that Hypothesis B and isotache framework work for both laboratory specimens and in situ soils with greater thickness and time scales.

CONCLUSIONS

This paper points out that the difference between Hypotheses A and B should be strictly to (1) whether creep serves as an independent phenomenon from the dissipation of excess pore water pressure or (2) whether the uniqueness concept of EOP void ratio-effective stress relationship stays true. Most existing EVP constitutive models are supportive of Hypothesis B. Although the introduction of an internal variable is what makes the MIT-SR model a different non-isotache model, when used properly for predicting the long-term consolidation behaviour of clay ($\beta \neq 0$), this model should align with Hypothesis B.

Inspired by Degago *et al*. (2011), historical data with discrepancies in verifying Hypothesis A or B, particularly the data documented by Watabe *et al*. (2008b), has been re-analysed using isotache framework. The following conclusions are summarized.

- The reassessment of the testing results from Watabe *et al*. (2008b) demonstrated the importance of equal initial conditions on the comparison between Hypotheses A and B. If Ma11 specimens were homogeneous and had no bedding error with equal initial void ratio, Hypothesis B would be verified.

Accepted manuscript doi:
10.1680/jgeot.23.00498

- Under different initial conditions of void ratio, isotache models could also interpret the experimental observations with compression behaviours that have previously been used to support Hypothesis A.
- The good agreement observed between the measured data and the simulation results using the methods associated with Hypothesis B underscores the validity and applicability of Hypothesis B for predicting the long-term consolidation behaviour of soft soil in both laboratory and field scales.

ACKNOWLEDGEMENTS

The work in this paper is supported by a Research Impact Fund (RIF) project (R5037-18), a Theme-based Research Scheme Fund (TRS) project (T22-502/18-R), and General Research Fund (GRF) projects (15231122 and 15226722) from Research Grants Council (RGC) of Hong Kong Special Administrative Region Government of China. The authors also acknowledge the financial supports from grants (ZDBS, CD7A, CD7A, CD82, BD8U) from Research Institute for Land and Space and from The Hong Kong Polytechnic University.

Accepted manuscript doi:
10.1680/jgeot.23.00498

Notations

C_c	compression index
C_k	coefficient for change of permeability
C_α	secondary compression coefficient
c_v	coefficient of consolidation
e	void ratio
e_0	initial void ratio
e_{0ave}	average initial void ratio
H	maximum drainage distance
k_{v0}	in situ coefficient of permeability
m_t	transient coefficient
n	soil porosity
R_a	internal strain rate
T_{99}	time factor corresponding to 99% degree of consolidation
t	elapsed time
t_p	duration of primary consolidation
t_{99}	time to achieve 99% degree of consolidation
V	specific volume
β	rate sensitivity
γ_w	unit weight of water

Accepted manuscript doi:
10.1680/jgeot.23.00498

ε	total strain
$\dot{\varepsilon}$	total strain rate
$\dot{\varepsilon}^{e}$	elastic strain rate
$\dot{\varepsilon}^{vp}$	viscoplastic strain rate
$\dot{\varepsilon}_{ref}$	reference strain rate
$\dot{\varepsilon}_{EOP}$	vertical strain rate at end of primary consolidation
κ	slope of un/reloading line
κ^{*}	modified swelling index
λ	slope of normally consolidation line
λ^{*}	modified compression index
μ^{*}	modified creep index
ρ_c	slope of the limiting compression curve in log(e)-log(σ'_v) space
ρ_r	slope of un/reloading line in log(e)-log(σ'_v) space
ρ_α	material constant for the creep behaviour
σ'_p	reference stress defined on limiting compression curve
σ'_v	effective vertical stress
σ'_{vi}	effective vertical stress caused by soil's self-weight
σ'_{pp}	notation used in this study to describe the pre-consolidation pressure in SSC model
$\bar{\sigma}'_p$	notation used in this study to describe the pre-consolidation pressure in Mesri's theory
τ	reference time

References

Augustesen, A., Liingaard, M., & Lade, P. V. (2004). Evaluation of time-dependent behavior of soils. *Int. J. Geomech*. **4**, No. 3, 137-156.

Aung, Y., Khabbaz, H., & Fatahi, B. (2019). Mixed hardening hyper-viscoplasticity model for soils incorporating non-linear creep rate–H-creep model. *Int. J. Plast.* **120**, 88-114.

Berre, T. & Iversen, K. (1972). Oedometer test with different specimen heights on a clay exhibiting large secondary compression. *Géotechnique* **22**, No. 1, 53-70.

Bjerrum, L. (1967). Engineering geology of Norwegian normally-consolidated marine clays as related to settlements of buildings. *Géotechnique **17***, No. 2, 83–118.

Canadian Geotechnical Society (2023). Canadian Foundation Engineering Manual. 5th Edition. Canadian Science Publishing.

Chen, Z. J., Feng, W. Q. & Yin, J. H. (2021). A new simplified method for calculating short-term and long-term consolidation settlements of multi-layered soils considering creep limit. *Comput. Geotech.* **138**, 104324.

Chen, Z. J., Feng, W. Q., Yin, J. H. & Shi, X. S. (2023). Finite element model and simple method for predicting consolidation displacement of soft soils exhibiting creep underneath embankments in 2-D condition. *Acta Geotech.* **18**, No. 5, 2513–2528.

Dadras-Ajirloo, D., Grimstad, G., & Amiri, S. A. G. (2023). On the isotache viscous modelling of clay behaviour using the hyperplasticity approach. *Géotechnique* **73**, No. 12, 1112-1124.

Dadras-Ajirlou, D., Grimstad, G., Ghoreishian Amiri, S. A., Degago, S. A., & Houlsby, G. T. (2024). Modified cam clay bounding surface hyper-viscoplastic model. *Géotechnique* **1**, No. 15.

Degago, S. A., Grimstad, G., Jostad, H. P. & Nordal, S. (2009). The non-uniqueness of the end-of-primary (EOP) void ratio-effective stress relationship. In *Proceedings of the 17th International Conference on Soil Mechanics and Geotechnical Engineering* (Volumes 1, 2, 3 and 4) (pp. 324–327). IOS Press.

Degago, S. A., Grimstad, G., Jostad, H. P., Nordal, S. & Olsson, M. (2011). Use and misuse of the isotache concept with respect to creep hypotheses A and B. *Géotechnique* **61**, No. 10, 897–908.

Feng, W. Q., Yin, J. H., Chen, W. B., Tan, D. Y. & Wu, P. C. (2020). A new simplified method for calculating consolidation settlement of multi-layer soft soils with creep under multi-stage ramp loading. *Eng. Geol.* **264**, 105322.

Funk, J. R. (2013). *Settlement of the Kansai International Airport Islands*. PhD thesis, University of Illinois at Urbana–Champaign, IL, USA.

Furudoi, T., & Kobayashi, M. (2009). Geotechnical issues and approach on Kansai International Airport Project—Prediction and performance of settlement. *J. Soc. Civ. Eng. Ser. C*, **65** No. 4, 998-1017.

Furudoi, T. (2010). The second phase construction of Kansai International Airport considering the large and long-term settlement of the clay deposits. *Soils Found*. **50** No. 6, 805-816.

Garlanger, J. E. (1972). The consolidation of soils exhibiting creep under constant effective stress. *Géotechnique* **22**, No. 1, 71–78.

Gheisari, N., Qi, S. & Simms, P. (2023). Incorporation of three different creep models into large-strain consolidation analysis of a clayey tailings deposit. *Comput. Geotech.* **161** 105533.

Grimstad, G., Dadrasajirlou, D., & Ghoreishian Amiri, S. A. (2020). Modelling creep in clay using the framework of hyper-viscoplasticity. *Geotech. Lett.* **1**, No. 3, 404-408.

Imai, G. & TANG, Y. (1992). A constitutive equation of one-dimensional consolidation derived from inter-connected tests. *Soils Found.* **32**, No. 2, 83–96.

Jamilkowski, M., Ladd, C. C., Germaine, J. T. & Lancellotta, R. (1985). New development in field and laboratory testing of soils. In *Proceedings of the 11th ICSMFE* Vol. 1, Balkema, Rotterdam, Netherlands, 57–153.

Ladd, C. C., Foott, R., Ishihara, K. & Schlosser, F. (1977). Stress-deformation and strength characteristics. In *Proceedings of the 9th International Conferenece on Soil Mechanics and Foundation Engineering*, Vol. 2, Japanese Society of Soil Mechanics and Foundation Engineering, Tokyo, 421–494.

Leroueil, S. (2006). Šuklje Memorial Lecture: The isotache approach. Where are we 50 years after its development by Professor Šuklje? In *Proceedings of the 13th Danube European Conference on Geotechnical Engineering*, Ljubljana 2, 55–88.

Levin, F., Vogt, S., & Cudmani, R. (2019). Time-dependent behaviour of sand with different fine contents under oedometric loading. *Can. Geotech. J.* **56** No. 1, 102-115.

Liu, Y. & Borja, R. I. (2022). Time scales in the primary and secondary compression of soils. *Int. J. Numer. Anal. Met. Geomech.* **46**, No. 8, 1383–1408.

Mesri, G. (1990). Discussion of 'Viscous-elastic-plastic modeling of one-dimensional time-dependent behavior of clays' by Yin & Graham (1989). *Can. Geotech. J.* **27** No. 2, 259–261.

Mesri, G. (2003). Primary and secondary compression. In *Soil behavior and soft ground construction* (eds J. T. Germaine, T. C. Sheahan and R. V. Whitman), Geotechnical Special Publication 119, pp. 122–166. Reston, VA: ASCE.

Mesri, G. & Choi, Y. K. (1985). The uniqueness of the end-of-primary (EOP) void ratio-effective stress relationship. In *Proceedings of the 11th International Conference on Soil Mechanics and Foundation Engineering, San Francisco* 2, 587–590.

Mesri, G. & Funk, J. R. (2015). Settlement of the Kansai international airport islands. *J. Geotech. Geoenviron. Engng.* **141** No. 2, 04014102.

Mesri, G. & Kane, T. (2018). Reassessment of isotaches compression concept and isotaches consolidation models. *J. Geotech. Geoenviron. Engng.* **144** No. 3, 04017119.

New Kansai International Airport Company (NKIAC). (2023). http://www.nkiac.co.jp (Aug, 2023).

Rocchi, G., Vaciago, G., Fontana, M. & Plebani, F. (2006). Enhanced prediction of settlement in structured clays with examples from Osaka Bay. *Geomech. Geoengin.* **1**, No. 3, 217–237.

Song, D. B., Lou, K., Chen, W. B., Wu, P. C., & Yin, J. H. (2024). Finite strain elastic visco-plastic consolidation model for layered soils with vertical drain considering self-weight loading and nonlinear creep. *Comput. Geotech.* **169**, 106180.

Šuklje, L. (1957). The analysis of the consolidation process by the isotache method. In *Proceedings of the 4th International Conference on Soil Mechanics and Foundation Engineering*, London (Vol. 1, pp. 200–206).

Szavits-Nossan, V. (2015). Consolidation and creep: Hypotheses A and B revisited. In *Proceedings of the XVI ECSMGE Geotechnical Engineering for Infrastructure and Development*, Edinburgh (pp. 3765–3770).

Vermeer, P. A. & Neher, H. P. (1999). A soft soil model that accounts for creep. *In Beyond 2000 in computational geotechnics: 10 Years of Plaxis International* (ed. R. B. J. Brinkgreve), pp. 249–261. Rotterdam: Balkema.

Watabe, Y., Tsuchida, T., & Adachi, K. (2002). Undrained shear strength of Pleistocene clay in Osaka Bay. *J. Geotech. Geoenviron. Engng*. **128**, No. 3, 216-226.

Watabe, Y., Udaka, K. & Morikawa, Y. (2008a). Strain rate effect on long-term consolidation of Osaka bay clay. *Soils Found.* **48**, No. 4, 495–509.

Watabe, Y., Udaka, K., Kobayashi, M., Tabata, T. & Emura, T. (2008b). Effects of friction and thickness on long-term consolidation behavior of Osaka Bay clays. *Soils Found.* **48**, No. 4, 547–561.

Watabe, Y., Udaka, K., Nakatani, Y. & Leroueil, S. (2012). Long-term consolidation behavior interpreted with isotache concept for worldwide clays. *Soils Found.* **52**, No. 3, 449–464.

Watabe, Y. & Leroueil, S. (2015). Modeling and implementation of the isotache concept for long-term consolidation behavior. *Int. J. Geomech.* **15**, No. 5, A4014006.

Yin, J. H. & Graham, J. (1989). Viscous–elastic–plastic modelling of one-dimensional time-dependent behaviour of clays. *Can. Geotech. J.* **26**, No. 2, 199–209.

Yin, J. H. (1999). Non-linear creep of soils in oedometer tests. *Géotechnique* **49**, No. 5, 699–707.

Yin, J. H. & Feng, W. Q. (2017). A new simplified method and its verification for calculation of consolidation settlement of a clayey soil with creep. *Can. Geotech. J.* **54**, No. 3, 333–347.

Yin, J. H. & Graham, J. (1994). Equivalent times and one-dimensional elastic viscoplastic modelling of time-dependent stress–strain behaviour of clays. *Can. Geotech. J.* **31** No. 1, 42–52.

Yin, J. H. & Graham, J. (1996). Elastic visco-plastic modelling of one-dimensional consolidation. *Géotechnique*, **46**, No. 3, 515–527.

Yin, J. H. & Zhu, J. G. (1999). Elastic viscoplastic consolidation modelling and interpretation of pore-water pressure responses in clay underneath Tarsiut Island. *Can. Geotech. J.* **36**, No. 4, 708–717.

Yin, J. H. & Zhu, G. (2020). *Consolidation analyses of soils*. CRC Press.

Yin, J. H., Chen, Z. J. & Feng, W. Q. (2022). A general simple method for calculating consolidation settlements of layered clayey soils with vertical drains under staged loadings. *Acta Geotech.* **17**, No. 8, 3647–3674.

Yuan, Y. (2016). *A new elasto-viscoplastic model for rate-dependent behavior of clays*. PhD thesis. Massachusetts Institute of Technology, MA, USA.

Yuan, Y. & Whittle, A. J. (2018). A novel elasto-viscoplastic formulation for compression behaviour of clays. *Géotechnique* **68** No. 12, 1044–1055.

Accepted manuscript doi:
10.1680/jgeot.23.00498

Tables

Table 1. Comparison among different models

Model	ILLICON approach	SSC model	1D MIT-SR
Hypothesis	A	B	B (when $\beta \neq 0$)
Assumptions	• Uniqueness of the EOP void ratio-effective vertical stress relationship • C_α/C_c law of compressibility	• Isotache framework	• Internal variable • Activation and decay function (equivalent to isotache model when steady state is reached)
Total strain rate composition	$\dot{\varepsilon} = \left(\frac{\partial \varepsilon}{\partial \sigma'_v}\right)_t \frac{\partial \sigma'_v}{\partial t} + \left(\frac{\partial \varepsilon}{\partial t}\right)_{\sigma'_v}$	$\dot{\varepsilon} = \dot{\varepsilon}^e + \dot{\varepsilon}^{vp}$ $\dot{\varepsilon}^e \approx \frac{\kappa^*}{2}\frac{\dot{\sigma}'_v}{\sigma'_v}$ $\dot{\varepsilon}^{vp} = \frac{\mu^*}{\tau}\left(\frac{\sigma'_v}{\sigma'_{pp}}\right)^{\frac{\lambda^*-\kappa^*}{\mu^*}}$	$\dot{\varepsilon} = \dot{\varepsilon}^e + \dot{\varepsilon}^{vp}$ $\dot{\varepsilon}^e = \rho_r n \frac{\dot{\sigma}'_v}{\sigma'_v}$ $\dot{\varepsilon}^{vp} = R_a \cdot \left(\frac{\sigma'_v}{\sigma'_p}\right)$ $\dot{\varepsilon}^{vp} = \frac{\rho_c - \rho_r}{\rho_c}\dot{\varepsilon}_{ref}\left(\frac{\sigma'_v}{\sigma'_p}\right)^{\frac{1}{\beta}}$ (steady state)
Parameters related to creep	C_α, t_p	μ^*, $\tau = 1$ day	R_{a0}, ρ_α, β, $\dot{\varepsilon}_{ref}$
Typical CRS behaviour	N.A.	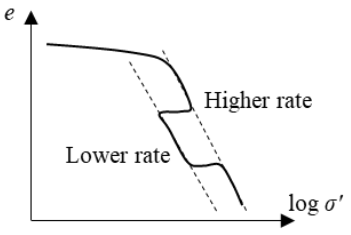	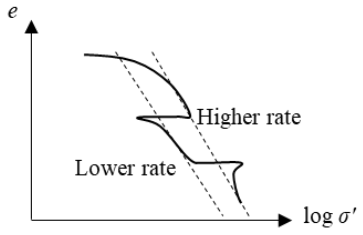

Accepted manuscript doi:
10.1680/jgeot.23.00498

Table 2. Soil parameters of Osaka clay Ma11 for different models

Yuan & Whittle, MIT-SR[1]	ρ_c	ρ_r	ρ_α	β	$\dot{\varepsilon}_{ref}$	σ'_{p0}
	0.30	0.035	0.012	0	N/A	700 kPa
Yuan & Whittle, MIT-SR[2]	ρ_c	ρ_r	ρ_α	β	$\dot{\varepsilon}_{ref}$	σ'_{p0}
	0.30	0.022	0.009	0.03	0.036 %/h	700 kPa
Vermeer & Neher, SSC[3]	λ^*	κ^*	μ^*	τ		POP[4]
	$\frac{0.3e_0}{1+e_0}$	$\frac{0.044e_0}{1+e_0}$	$\frac{0.009e_0}{1+e_0}$	1day		720 kPa

Notes:

1. Soil parameters from Yuan and Whittle (2018) for predicting Hypothesis A behaviour
2. Soil parameters from Yuan and Whittle (2018) for predicting Hypothesis B behaviour, which were also adopted to simulate the long-term consolidation tests on H2, H10, and H20 in this study.
3. $\kappa^* \approx \frac{2\kappa}{1+e_0} = \frac{2\rho_r e_0}{1+e_0}$, modified swelling index; $\lambda^* = \frac{\lambda}{1+e_0} = \frac{\rho_c e_0}{1+e_0}$, modified compression index; $\mu^* = \frac{\rho_\alpha e_0}{1+e_0}$, modified creep index, σ'_{v0} =489 kPa, C_k = 1.15, k_{v0} = 2.55×10^{-10} m/s. The values of e_0 are presented in Fig. 4.
4. POP= 720 kPa is the reference pressure of preconsolidation according to the average initial void ratio e_{0ave} of each specimen. For different values of initial void ratio e_0, the values of POP need to be updated (Fig. 6)

Table 3. Values of POP and corresponding initial void ratio of specimens H2, H10, and H20

Specimen	Specimen element	Initial void ratio	Updated value of POP (kPa)
H2	1	1.2267	727
	2	1.2330	713
H10	1	1.3102	607
	2	1.2146	814
	3	1.2390	752
	4	1.2654	692
	5	1.2346	763
H20	1	1.2836	738
	2	1.2842	737
	3	1.3106	681
	4	1.3165	669
	5	1.2691	772
	6	1.2642	784
	7	1.2721	765
	8	1.3082	685
	9	1.2940	715
	10	1.3151	672

Table 4. Soil parameters of Osaka clay Ma11 at MP1-II of the Kansai International Airport

Sublayer	Thickness (m)	e_0	λ^*	κ^*	μ^*	k_{v0} n/s)	C_k	σ'_{v0} [1] (kPa)	POP[2] (kPa)
Ma11U1	6.5	.565	0.1830	0.0210	0.00732	5.5×10^{-10}	.78	530	758
Ma11U2	4.3	.083	0.1560	0.0182	0.00624	2.3×10^{-10}	.54	560	801
Ma11L	9.8	.480	0.1790	0.0209	0.00716	7.6×10^{-10}	.74	630	901

Notes:

1. σ'_{v0} is the initial effective vertical stress at the middle level of each sublayer of Ma 11. Values of σ'_{v0} were determined based on the data from Funk (2013).
2. $\text{POP} = \text{OCR} \times \sigma'_{v0}$, OCR = 1.43 was used for all sublayers of Ma 11.

Figure captions

Fig. 1. Illustration of Hypotheses (Curves) A and B for samples with equal initial conditions and under the same effective stress increment (after Ladd *et al*., 1997 and Jamiolkowski *et al*., 1985)

Fig. 2. Illustration of MIT-SR model proposed by Yuan and Whittle (2018) and SSC model proposed by Vermer & Neher (1999)

Fig. 3. Average strain-log(time) curves of specimens with different thicknesses from the long-term consolidation tests on Osaka clay Ma11: (a) incremental average strain and (b) absolute average strain

Fig. 4. (a) Relationship between e_0 of different specimen elements and the maximum drainage distances H and (b) void ratio change Δe at EOP and initial void ratio e_0 of Osaka clay Ma11

Fig. 5. Relationship between $\Delta e / e_0$ at EOP and thickness of Osaka clay Ma11

Fig. 6. Illustration of the relationship between initial void ratio and pre-consolidation pressure

Fig. 7. Simulation results of Osaka clay Ma11 using SSC model and MIT-SR model: (a) actual initial void ratios for different specimens and (b) identical initial void ratio for all specimens

Fig. 8. Illustration of the soil profile at MP1-II and the numerical model of Ma 11 layer in PLAXIS

Fig.9 (a) Simplified load at seabed $\Delta\sigma_v'$ and (b) compression of Ma11 layer at MP1-II

Fig. 10. Calculated and measured surface settlement of embankments over soft soils or compression of soft soil at the end of observation

Accepted manuscript doi:
10.1680/jgeot.23.00498

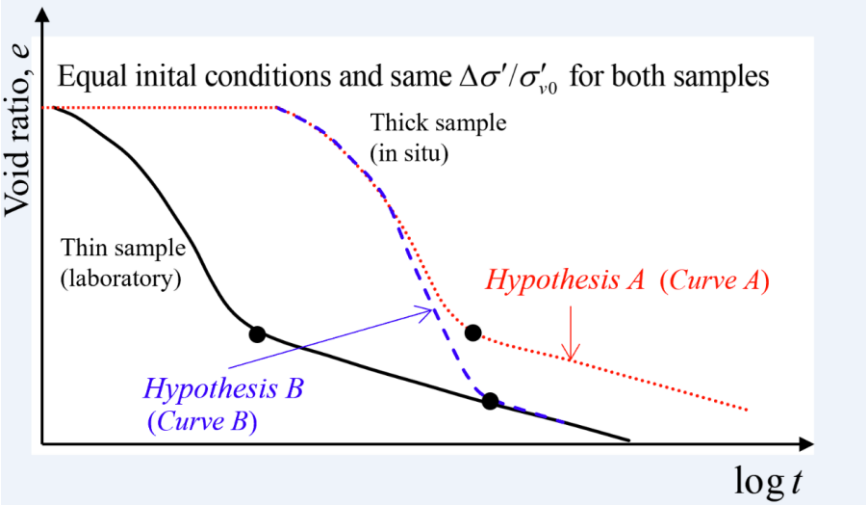

Fig. 1

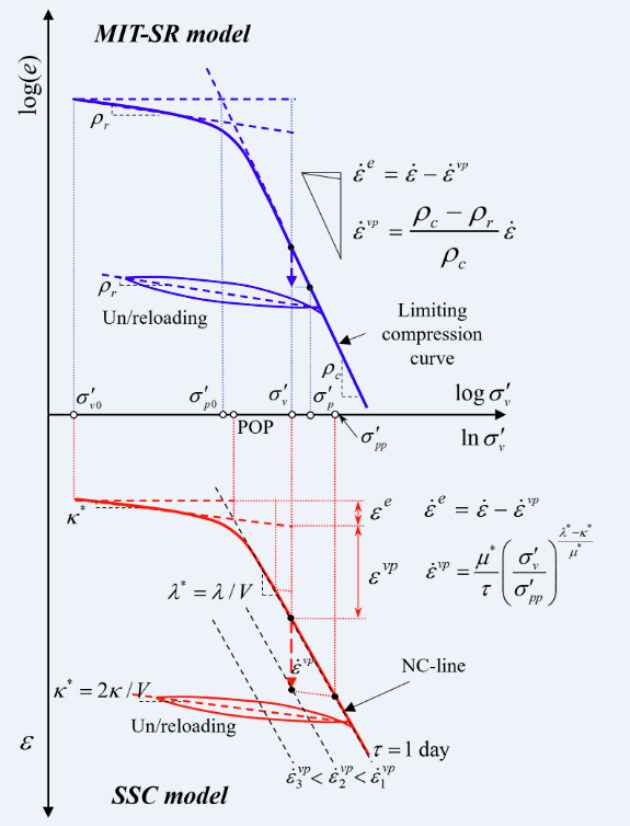

Fig. 2

Accepted manuscript doi:
10.1680/jgeot.23.00498

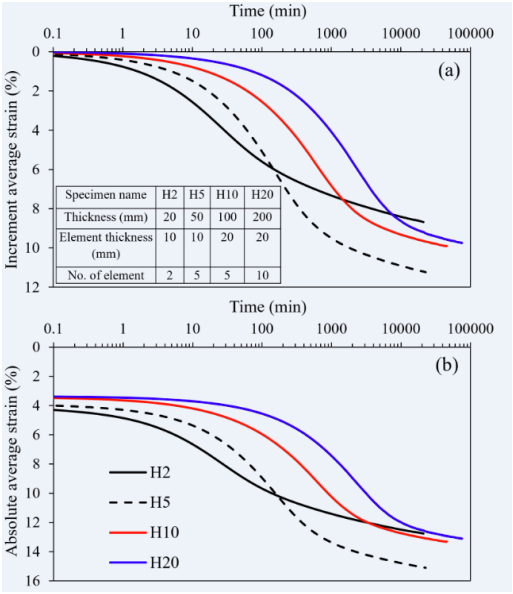

Fig. 3

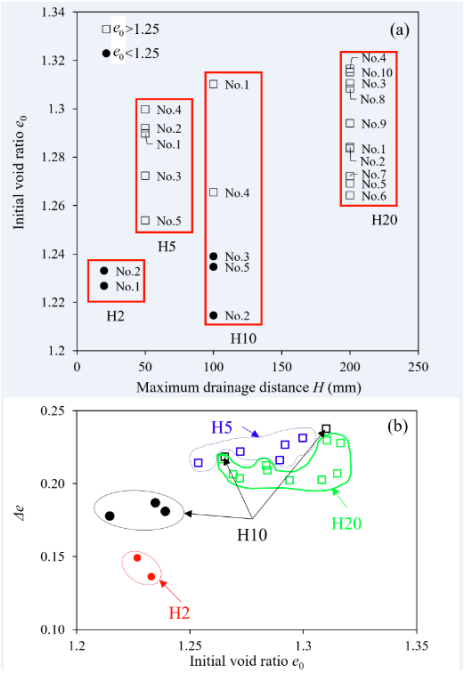

Fig. 4

Accepted manuscript doi:
10.1680/jgeot.23.00498

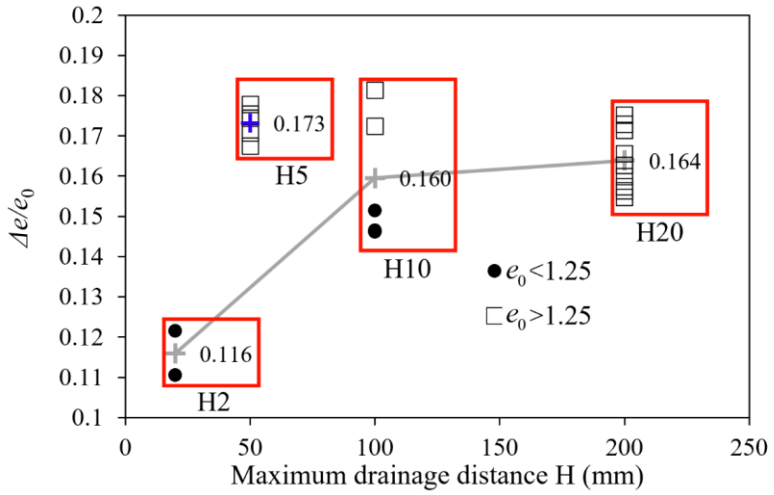

Fig. 5

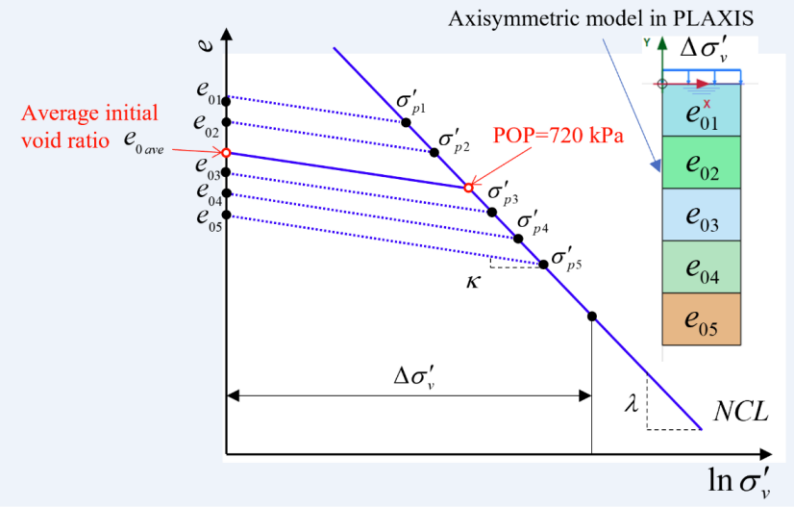

Fig. 6

Accepted manuscript doi:
10.1680/jgeot.23.00498

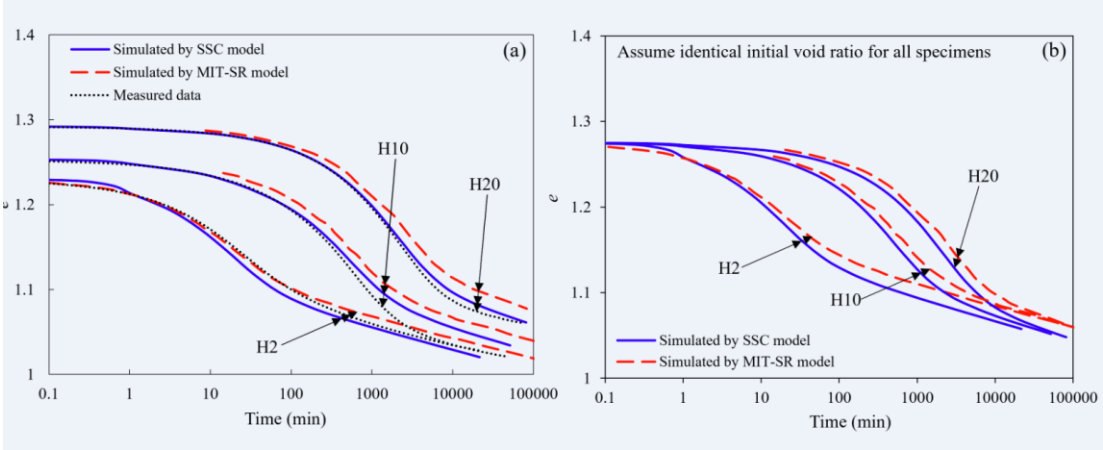

Fig. 7

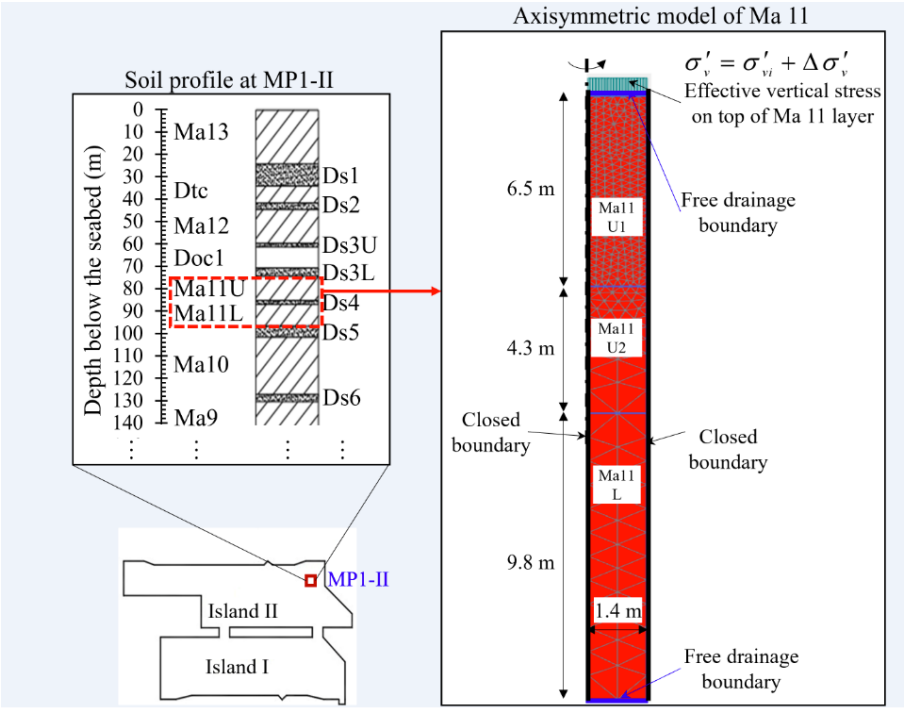

Fig. 8

Accepted manuscript doi:
10.1680/jgeot.23.00498

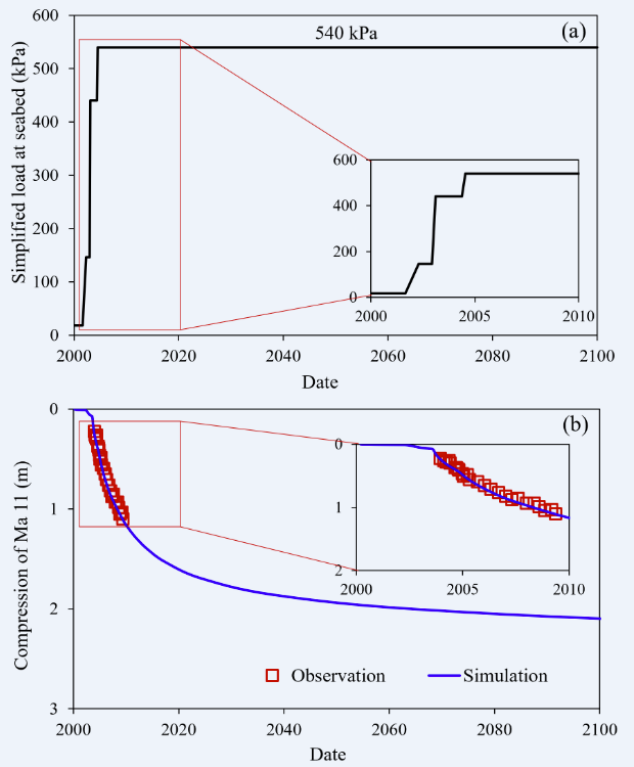

Fig. 9

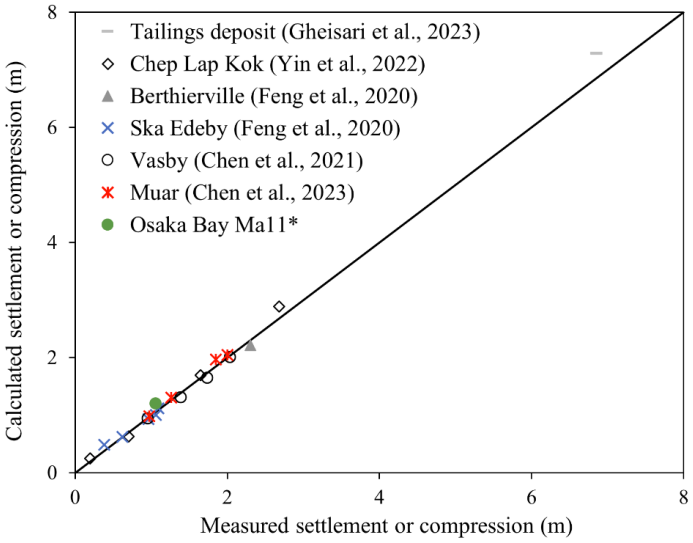

Fig. 10